

## Computation of the ultraviolet absorption and electron inelastic scattering cross section of multishell fullerenes

A. A. Lucas, L. Henrard, and Ph. Lambin

*Institute for Studies in Interface Sciences, Facultés Universitaires Notre-Dame de la Paix, 61 rue de Bruxelles, B5000 Namur, Belgium*

(Received 12 July 1993; revised manuscript received 12 October 1993)

We develop a model in which the ultraviolet dielectric tensor of planar graphite is transported to the spherical geometry of a nanoscale multishell fullerene with a central cavity. This is accomplished by assigning to every point of the multishell fullerene a local dielectric tensor identical to that of graphite with its  $c$  axis aligned along the local radial direction. The dynamic, multipolar polarizabilities of the model fullerene are obtained from the exact solutions of the nonretarded Maxwell equations. The ultraviolet absorption spectrum of the hollow fullerene is calculated as a function of the ratio of the inner and outer radii. Comparisons of the theoretical absorption spectra with the 2175-Å interstellar extinction hump and with recent absorption measurements for synthetic multishell fullerenes indicate that the dielectric properties of graphite are qualitatively adequate for understanding the optical data. However, difficulties persist with both the astrophysical and laboratory absorption peaks which lead us to consider the possible role of multishell fullerene aggregation into small or large clusters. It is found that the effect of clustering is important and reduces but does not remove completely the quantitative difficulties of the graphitic multishell model. Finally theoretical electron-energy-loss spectra (EELS) of these structures with an empty or filled cavity are calculated from the multipolar polarizabilities of the model. The results indicate that spatially resolved EELS measurements should be ideally suited to study the dielectric properties of individual multishell fullerenes and to ascertain to what extent they differ from those of planar graphite.

### I. INTRODUCTION

The recent discovery of the closed-cage fullerene molecules  $C_n$  (Refs. 1 and 2) has precipitated several surprising observations in the science of pure-carbon materials. Transmission electron microscopy<sup>3-6</sup> (TEM) has revealed that multishell fullerenes of tubular or globular shapes can grow under a large variety of conditions. Such particles constitute highly stable forms of pure-carbon clusters down to the nanoscopic and angstrom size range: the formation of curled-up, multilayer particles appears to be energetically favored in the growth process because of the elimination of the dangling bonds by closure of the graphene sheets.<sup>7</sup> Thus, perfectly spherical, multishell fullerenes have been observed by Ugarte<sup>6</sup> to form under a high dose of energetic electrons in TEM. The exceptional stability of these structures suggests the possibility<sup>6</sup> that the spheroidal graphite particle might represent the ultimate form of carbon nanoclusters most resistant to disorder in a large variety of harsh but chemically inert conditions.

Soon after their discoveries, it was speculated<sup>8</sup> that fullerene molecules and multishell fullerenes are present in interstellar space as constituents of carbon-containing dust or meteorites<sup>4,9</sup> (one should remember that it was the study of interstellar carbon which led to the serendipitous discovery of the fullerenes in the laboratory<sup>1,2</sup>). A necessary condition for proving the existence of fullerenes in space is that their optical properties be found consistent with those of interstellar dust in the galaxy, most particularly the ubiquitous broad absorption band

at 2175 Å (5.7 eV,  $4.6 \mu\text{m}^{-1}$ ), which is believed to originate in the graphitic carbon content of the dust.<sup>1,11</sup> A strong contribution to this band from the most stable, monolayer fullerenes  $C_{60}$  and  $C_{70}$  appears to be excluded by the observation that these molecules have a characteristic doublet absorption in this energy region (the so-called camel spectrum),<sup>2</sup> whereas the observed band has a single peak. Regarding the possible contribution of carbon multishells, as no laboratory data existed until very recently, several theoretical models had already been constructed<sup>12-15</sup> to compare their ultraviolet spectrum with the interstellar hump. The model that we proposed<sup>14</sup> consisted of a hollow spherical shell with adjustable inner and outer radii and with dielectric properties transported from planar graphite and adapted to the spherical geometry. This model gave encouraging but not completely satisfactory results: while the hollow multishell model reproduced the interstellar peak position and average width quite accurately, it did not provide an explanation for the lack of correlation between the fixed hump position and the variable hump widths in different lines of sight in the galaxy.<sup>14</sup>

Very recently, de Heer and Ugarte<sup>16</sup> succeeded in preparing multishell samples in an amount sufficient for a direct measure of their ultraviolet absorption when suspended in water. A broadband was obtained with a spectral shape similar to the interstellar hump. Particularly significant for the discussions of the present paper were the observations that (i) practically all nanoscopic multishells prepared by heat treatment were indeed hollow and (ii) while the absorption bandwidth varied with

the sample heat treatment, the peak position remained essentially constant.

In the light of these results, which are highly significant for the interstellar dust problem, we wish to reconsider the theoretical model introduced in Ref. 14 and interpret the new laboratory data<sup>16</sup> from it. We find that the multishell model with graphitic dielectric properties is qualitatively justified. However, there remain features which cannot be fully explained from the properties of *isolated* multishells, namely, a systematic redshift of the observed peak and the same uncorrelated width characteristic of the interstellar hump. We show that both of these effects are likely due, at least partly, to the average effect of multishell clumping in the water suspension.

Finally, the same model is used here to make predictions for possible results obtained by electron-energy-loss spectroscopy (EELS) of graphitic multishells with empty or filled inner cavities. Such a spectroscopy could indeed be used in the future to explore the spatially resolved excitations of one single hollow multishell throughout the energy range from the infrared to the far ultraviolet.<sup>17</sup> Such an investigation would be invaluable in ascertaining more precisely the transferability of graphite properties to curved carbon structures of nanoscopic radii.

## II. DIELECTRIC MODEL

The spherical shell morphology of nanoscopic-size multishells precludes the use of the highly anisotropic optical properties of planar graphite in the way customarily applied to small graphite spheres, namely, by simply averaging over the three possible directions of the  $c$  axis with respect to the electric field.<sup>18</sup> It is necessary to solve the Maxwell equations and the associate boundary conditions for the actual, spherical anisotropy of the multishell. This turns out to be an exercise in classical electrodynamics that is especially straightforward when the nonretarded approximation is applicable, as is the case here for multishells of outer radii  $R$  ( $\sim 10$  nm) much smaller than the wavelengths of interest ( $\lambda \sim 100$  nm).

Referring to Fig. 1(a), we write the continuum, uniaxial graphite dielectric tensor as

$$\epsilon(\omega) = \epsilon_{\perp}(\omega)(\mathbf{x}\mathbf{x} + \mathbf{y}\mathbf{y}) + \epsilon_{\parallel}(\omega)\mathbf{z}\mathbf{z}, \quad (1)$$

where the unit vector  $\mathbf{z}$  coincides with the graphite  $c$  axis and  $\mathbf{x}, \mathbf{y}$  are orthogonal unit vectors parallel to the graphite sheets. The principal components  $\epsilon_{\perp}(\omega)$  and  $\epsilon_{\parallel}(\omega)$  have been measured by several methods which unfortunately do not fully agree throughout the UV spectral range.<sup>19</sup>

We now transfer  $\epsilon(\omega)$  to the spherical multishell of Fig. 1(b) by assuming that the multishell material is also a dielectric continuum, locally identical to graphite. At every point, we simply write a local dielectric tensor taken from Eq. (1) where  $\mathbf{x}, \mathbf{y}$ , and  $\mathbf{z}$  are replaced by the local unit vectors  $\mathbf{r}, \boldsymbol{\theta}$ , and  $\boldsymbol{\phi}$  of the spherical coordinates [Fig. 1(b)]:

$$\epsilon(\mathbf{r}, \omega) = \epsilon_{\perp}(\omega)(\boldsymbol{\theta}\boldsymbol{\theta} + \boldsymbol{\phi}\boldsymbol{\phi}) + \epsilon_{\parallel}(\omega)\mathbf{r}\mathbf{r}. \quad (2)$$

This procedure becomes rigorous when the internal ra-

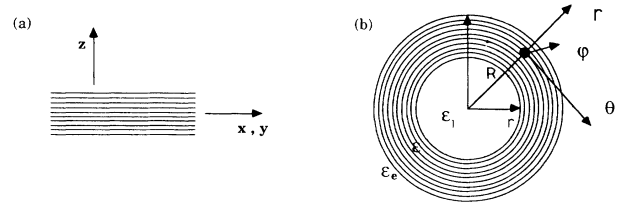


FIG. 1. Dielectric model for (a) graphite and (b) graphitic multishells. The dielectric tensor of graphite, which is diagonal in the Cartesian coordinates in (a), is transposed to the spherical geometry of model (b) as explained in the text.

dius  $r$  of the multishell is very much larger than the multishell interlayer distance  $c_0 \sim 3.4$  Å (about the same as in planar graphite<sup>6</sup>). Clearly, for  $r$  not much larger than  $c_0$ , atomistic effects are likely to bring about modifications in the dielectric function such as a nonlocal character, radial inhomogeneity, extra damping, etc. Note that a major part of the nonlocality, i.e., that arising from the curvature, is already incorporated in the mere writing of Eq. (2). Additional, plausible radial dependencies  $\epsilon_{\perp}(r, \omega)$ ,  $\epsilon_{\parallel}(r, \omega)$  and enhanced damping could easily be introduced in the model if empirical data were to make such refinements necessary. Angular nonlocality associated with the atomicity of the individual multishell layers is, however, outside the scope of the present model. For simplicity, in this paper we shall rigidly transfer the local dielectric constants as indicated in Eqs. (1) and (2).

We further assume that the multishell may be hollow [inner radius  $r$ ; see Fig. 1(b)], possibly contain a second material, and be surrounded by a third material. These internal and external media will be taken to be isotropic and homogeneous continua with local dielectric functions  $\epsilon_i(\omega)$  and  $\epsilon_e(\omega)$ , respectively. This will be useful in interpreting the observations of UV absorption of multishells suspended in water<sup>16</sup> and also in calculating optical properties of hollow graphitic multishells formed around amorphous carbon or metallic cores.<sup>20</sup>

## III. MULTIPOLAR POLARIZABILITIES

In the nonretarded approximation, it suffices to solve Gauss's equation  $\text{div}[\epsilon(\mathbf{r})\mathbf{E}(\mathbf{r})] = 0$  for the irrotational electric field  $\mathbf{E} = -\text{grad}V(\mathbf{r})$  and to impose the usual boundary conditions. The spherical symmetry of the problem dictates that one write the solution in terms of a spherical harmonics  $V(r)Y_{lm}(\theta, \phi)$ . The radial equation for  $V(r)$  is then easily found to be

$$r^2 d^2 V / dr^2 + 2r dV / dr - (\epsilon_{\perp} / \epsilon_{\parallel}) l(l+1) V = 0. \quad (3)$$

This will be formally identical to the radial equation of the completely isotropic problem if we introduce the effective azimuth quantum number  $u$  defined via

$$u(u+1) = (\epsilon_{\perp} / \epsilon_{\parallel}) l(l+1).$$

Therefore, the general solution within the multishell is  $Br^{u+} + Cr^{u-}$ , where  $B$  and  $C$  are integration constants and where

$$u_{\pm} = \frac{1}{2} \{ -1 \pm [1 + 4l(l+1)\epsilon_{\perp} / \epsilon_{\parallel}]^{1/2} \}. \quad (4)$$

Inside and outside the multishell, the regular solutions are  $Ar^l$  and  $Dr^{-(l+1)}$ , respectively, with  $A$  and  $D$  two new constants.

We impose the conditions that  $V(r)$  and  $\epsilon_{\parallel}dV(r)/dr$  be continuous at the outer ( $R$ ) and inner ( $r$ ) interfaces, and the compatibility condition of the resulting set of homogeneous equations gives the dispersion relation of the nonretarded excitations, given a set of dielectric functions. We want here to obtain the multipolar polarizabilities  $\alpha_l(\omega)$  of the multishell when subject to an external

electric field  $\mathbf{E}_{\text{ext}}(\mathbf{r})e^{-i\omega t}$ . We then need to add to the outside potential an inhomogeneous term corresponding to the  $l$ th multipolar order of the external excitation. For  $l=1$ , for instance, the external potential is

$$V_{\text{ext}} = -E_0 z = -E_0 r \cos\theta$$

and the term  $-E_0 r$  is added to the outside  $l=1$  radial potential. The dipole polarizability of the multishell is then given by  $-4\pi\epsilon_0 A/E_0$ . For an arbitrary  $l$ , the result of that cumbersome algebra is found to be

$$\alpha_l = 4\pi\epsilon_0\epsilon_e R^{2l+1} \frac{(\epsilon_{\parallel}u_- - l\epsilon_i)(\epsilon_{\parallel}u_+ - l\epsilon_e) - \rho(\epsilon_{\parallel}u_+ - l\epsilon_i)(\epsilon_{\parallel}u_- - l\epsilon_e)}{(\epsilon_{\parallel}u_- - l\epsilon_i)[\epsilon_{\parallel}u_+ + (l+1)\epsilon_e] - \rho(\epsilon_{\parallel}u_+ - l\epsilon_i)[\epsilon_{\parallel}u_- + (l+1)\epsilon_e]}, \quad (5)$$

where

$$\rho = (r/R)^{u_+ - u_-}. \quad (6)$$

Obviously, the multishell multipolar polarizabilities are scalar due to the spherical rotational invariance of the model. Equation (5) reduces to all the well-known electrostatic formulas for particular situations such as the plain ( $r=0$ ) isotropic sphere ( $\epsilon_{\perp} = \epsilon_{\parallel}$ ) and the hollow isotropic shell in vacuum ( $\epsilon_i = \epsilon_e = 1$ ).<sup>18</sup>

Alternatively, the ‘‘external’’ source field could be applied from the interior of the multishell, e.g., by the passage of a charged particle or by the fluctuating field of an atom trapped in the cavity. In that case, the same set of equations can be used to compute such quantities as the monopolar and multipolar responses of the multishell to the presence of the charged particle or the shift and broadening of the energy levels of an endohedral atom.<sup>21</sup>

## IV. UV ABSORPTION

### A. Calculations

If carbon multishells were present in interstellar dust, they would contribute to the stellar excitation in proportion to their relative abundance and their scattering and absorption cross sections. For particles of nanoscopic sizes ( $R \sim 100 \text{ \AA}$ ) such as those considered in this paper, scattering in the UV is negligible<sup>18</sup> and the contribution to the stellar extinction curve is dominated by absorption. The absorption cross section is directly given by the imaginary part of the dipole dynamic polarizability of the multishell according to

$$\sigma = (\omega/\epsilon_0 c) \text{Im}\alpha_{l=1}(\omega). \quad (7)$$

The cross section divided by the outer geometrical cross section defines the absorption efficiency  $Q = \sigma/\pi R^2$ .  $Q(\omega)$  shows a resonance around 6 eV for hollow multishells in vacuum.<sup>14</sup> The peak is attributable to the  $\pi$ -plasmon resonance in  $\epsilon_{\perp}$  of graphite at this energy.

From the formal results contained in Eqs. (5) and (6), the important geometrical parameter which controls the spectrum appears to be the  $r/R$  ratio, whereas the external radius  $R$  merely controls the absolute absorption strength. The presence of the cavity has an important

effect:<sup>14</sup> thinner shells tend to have their peak positions redshifted and to have narrower peaks. Figure 2 illustrates the dependence of the peak position and width on  $r/R$ . By definition, the former is the first moment of the absorption spectrum between 3 and 9 eV and the latter is the full width at half maximum of the peak.

The dielectric functions of the graphite used in the present calculations are those proposed by Draine and Lee.<sup>19</sup> There is no fundamental difference between this figure and Fig. 4 of Ref. 14 where Klucker’s dielectric functions were used. The position of the absorption peak is indeed controlled by the vanishing of the real part of  $\epsilon_{\perp}(\omega)$  around 6 eV and all the authors agree in their measurements of this component. For that reason, the peak position is not too sensitive to the particular set of dielectric data used in the calculations. For instance, the plateau in the curve of the peak position for small  $r/R$  ratios is shifted upwards by only 0.2 eV in the present calculations, and as  $r/R$  increases, the curve of Fig. 2(a) comes even closer to that in Ref. 14. Considering the simplicity

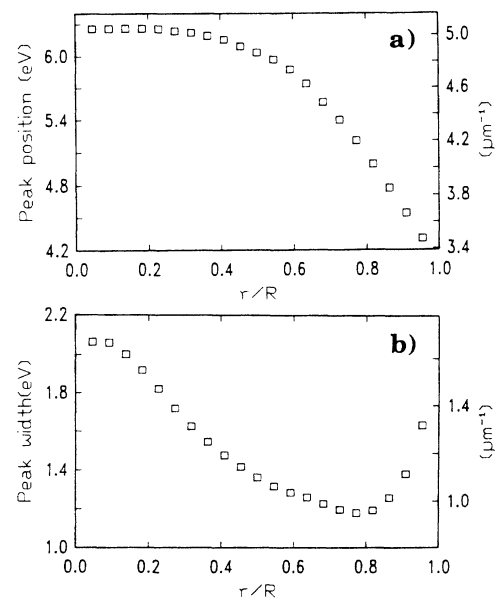


FIG. 2. The (a) position and (b) width of the absorption peaks of graphitic multishells are plotted against the ratio  $r/R$  of the internal and external radii of the dielectric shell model.

of the model, we do not regard this uncertainty in the position of the peak as a severe limitation of our approach. As for the width of the peak, its calculation involves the imaginary parts of both  $\epsilon_{\perp}$  and  $\epsilon_{\parallel}$  which are mixed in the absorption by the effects of the multishell curvature. Since  $\text{Im}(\epsilon_{\parallel})$  shows no particular features in the 6-eV region in the two experimental determinations under discussion here, the two sets of dielectric data lead to the same general behavior of the width of the absorption resonance of the multishells. The rise of the peak width for small values of  $r/R$  (thin multishells) is not an intrinsic property of the present continuum model but results from the peculiar behavior of the graphite dielectric tensor.

Let us stress that the increasing redshift predicted for thinner shells [Fig. 2(a)] arises from an enhanced coupling of the  $\pi$ -plasmon density fluctuations on the inner and outer surfaces of the hollow multishell. This is the spherical version of the redshift observed for the optically active surface plasmon in thin planar films when the film thickness decreases. Notice that, in an isotropic dielectric, one could expect two distinct dipolar modes, associated with, respectively, tangential and radial density fluctuations<sup>22,23</sup> [both of which are optically active on a sphere while only the "radial" mode (i.e., transverse to film) is active in a film<sup>25</sup>]. However, these modes cannot be so easily isolated in the anisotropic case and, moreover, such fine structure turns out to be smoothed out by damping effects.

### B. The interstellar hump

The present calculations of the absorption efficiency of the multishells reproduce the *average* interstellar absorption around 2175 Å quite well, as was already the case with Klucker's dielectric data.<sup>14</sup> It has been stressed<sup>26</sup> that while there are large variations ( $\pm 25\%$  of the average) in the absorption peak width from star to star, the peak position remains independent of the line of sight to within less than 1%. Figures 2(a) and 2(b), however, predict that in the 5.7-eV region, there are substantial correlated variations in both position and width when the ratio  $r/R$  is changed. If we therefore attempt to attribute the hump to multishells with a cavity size which is fine tuned to the peak position, we shall fail to account for the variations of the peak width (see Ref. 14 for a discussion).

In view of these conflicting results, and if the transferability of graphite properties proves correct, one cannot conclude that nanoscopic-size multishells are an important constituent of interstellar dust, at least as isolated particles. We shall see below that the contradictions are somewhat eased, but not completely removed, by the effects of multishell aggregation. Alternatively, if nanoscopic multishells prove to be abundant enough to dominate the hump, their strong curvature must alter the dielectric functions of planar graphite to the extent of invalidating the present rigid transfer procedure. To resolve the issue, one will need further laboratory data on the UV absorption of nanoscopic carbon particles of the large fullerene family. One notes that  $C_{60}$  fullerite shows two split absorption peaks at 4.8 and 5.8 eV (Refs. 2 and 25) of about equal strengths, averaging to 5.3 eV. This could be an indication that the most strongly curved, in-

nermost multishell layers will tend to have their  $\pi$ -plasmon excitations strongly shifted downwards from the 6.2-eV plateau region of Fig. 2(a) characteristic of the properties of planar graphite. If this were confirmed by experiment for multishell fullerenes, then the plateau region for multishell fullerenes, then the plateau region for small plain or nearly plain multishells would occur closer to the 5.7-eV interstellar peak than predicted here, thereby eliminating much of the peak-position variation while maintaining variable width.

Furthermore, the variation of the width of the absorption efficiency by interstellar dust for different lines of sight would have to be associated with different growth conditions and the chemical composition of the environment.<sup>24</sup> De Heer and Ugarte's data which are discussed below<sup>16</sup> have shown that the annealing temperature of carbon soot does influence the inner and outer radius and the shape of the multishells as well.

### C. Laboratory data

Recently, de Heer and Ugarte<sup>16</sup> have succeeded in producing macroscopic amounts of multishells with a relatively monodispersed distribution in the few-nanometer-size range. By contrast to the plain, well-ordered spherical particles formed under TEM electron irradiation,<sup>6</sup> the multishells produced by heat treatment of carbon soot in an inert atmosphere<sup>16</sup> were found to be *systematically hollow* and presented a generally globular, but polyhedral, structure. Their average ratio  $r/R$  appears to lie within rather narrow bounds. For instance, a visual inspection of Fig. 1(d) of Ref. 16 indicates an average ratio between 0.5 and 0.7. The visible-UV absorption spectra of suspensions of this material in water<sup>16</sup> revealed a  $\pi$ -plasmon band quite similar to the  $4.6\text{-}\mu\text{m}^{-1}$  interstellar feature, albeit with a peak position at  $3.8\text{ }\mu\text{m}^{-1}$ . Curve (a) in Fig. 3 shows one such spectrum. The heavy redshift was due in part to the water environment and, indeed, correction for the water dielectric constant brought the absorption peak to  $4.3\text{ }\mu\text{m}^{-1}$  as discussed

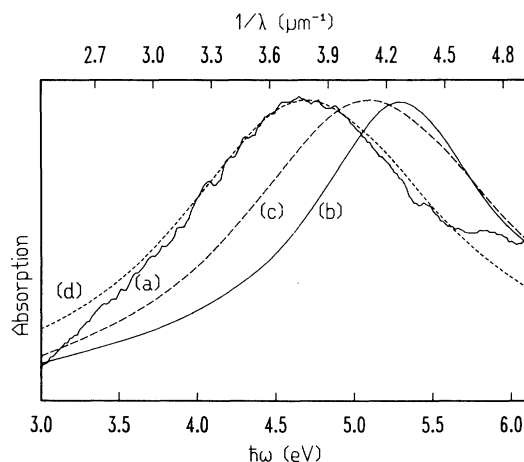


FIG. 3. (a) Solid curve: experimental UV absorption spectrum of a suspension of multishell particles in water (Ref. 16). (b) Theoretical absorption efficiency of an isolated multishell in water for  $r/R = 0.6$ . (c) Absorption efficiency of a compact aggregate of hyperfullerenes in water for the same  $r/R$  ratio. (d) Dotted curve: same as (c), shifted by  $0.32\text{ }\mu\text{m}^{-1}$ . A linear background has been added to the computed spectra (b)-(d).

below. The peak position in this and other samples was found to be fairly constant, but the peak width could vary from sample to sample, depending on the average number of layers in the multishell. These results are obviously of extreme interest for discussing the interstellar dust problem. In particular, they make it possible to confront anew the predictions of carbon dust models with new laboratory data.

Notwithstanding the polyhedral appearance of the multishells in Fig. 1(d) of Ref. 16, we believe that our spherically uniaxial model does capture the essential effect of their globular, concentric layer structure. In Fig. 3 we compare the prediction of this model [curve (b)] with the experimental spectrum [curve (a)] (Ref. 16) for a suspension of multishells in water. In the application of Eqs. (5) and (6), we took  $\epsilon_i = 1$  (empty cavity) and  $\epsilon_e = \epsilon_{\text{water}}$  as tabulated in Ref. 27 in the energy range under consideration.

A linear background was added to the multishell absorption efficiency  $Q(\omega)$  to represent an unknown proportion of residual raw soot and glassy carbon particles in the suspension.<sup>16</sup> The parameters for curve (b) in Fig. 3 were adjusted so as to best reproduce the observed peak strength and the overall increase in absorption towards the vuv. The theoretical absorption efficiency  $Q(\omega)$  is computed for  $r/R = 0.6$  as directly averaged from a visual sampling of the multishells in Fig. 1(d) of Ref. 16. One sees that the predicted efficiency [curve (b)] peaks at higher energy and is somewhat narrower than the experimental curve [curve (a)]. This residual redshift and broadening are tentatively assigned to the effect of particle clumping in the water suspension, as explained below.

Before we discuss the effects of the multishell clustering in Sec. V, let us return to the background of the spectra of Fig. 3 which was attributed to additional absorption by soot fragments and amorphous carbon particles in the suspension. Since the dielectric function of glassy carbon has been measured,<sup>28</sup> we can use the electrostatic model to evaluate the contribution of such amorphous particles. In Fig. 4 we compare the absorption efficiency

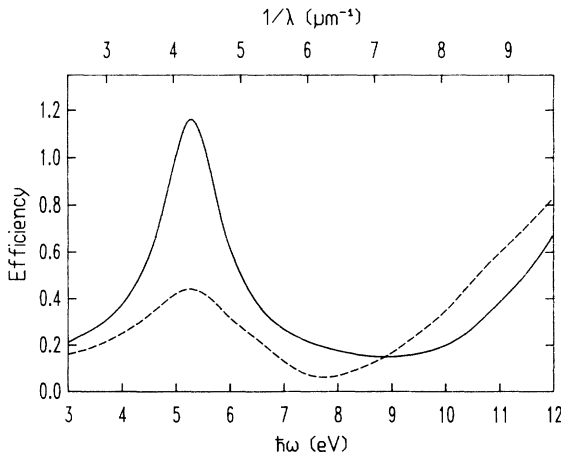


FIG. 4. The absorption efficiency of a graphitic multishell ( $r = 60 \text{ \AA}$ ,  $R = 100 \text{ \AA}$ ) in water (solid curve) is compared with the absorption of a spherical, glassy carbon particle (dashed curve) having the same external radius.

of our  $100\text{-\AA}$  hollow multishell ( $r/R = 0.6$ ) with that of a plain spherical, amorphous particle of the same outer radius. Due to the more pronounced  $sp^3$  character of the bands in glassy carbon, the multishell is four to five times more efficient in the  $\pi$ -plasmon region. The amorphous carbon particles, as well as the original soot fragments, are expected to have all sorts of irregular shapes which should further smear out their  $\pi$ -plasmon hump and contribute a rather smooth background.

## V. MULTISHELL CLUMPING

Clustering of the multishell material is likely to subsist in water suspension where neither the water dielectric screening nor the applied ultrasonic dispersion<sup>16</sup> seem sufficient to break the relatively strong (van der Waals) adhesion bonds between the particles (it should be remembered that  $C_{60}$  fullerite is already solid at room temperature with a 1.6-eV binding energy per molecule<sup>22</sup>). Since particle clumping originates from van der Waals forces and since the latter stem from the shift of the UV energy levels caused by the interparticle electron-electron interactions, clustering should be accompanied by changes in the frequencies of the optically active transitions. In a description of the particles in terms of harmonic oscillators, the van der Waals interaction energy<sup>31</sup> results from a lowering of the zero-point energy of the oscillators. It is then obvious that there must be an overall redshift of UV absorption frequencies. We thus attempt to interpret the residual frequency misfit in Fig. 3 between curves (a) and (b) as a particle clumping effect.

Unfortunately, the statistical distribution of cluster shapes and sizes in the experiment<sup>16</sup> is unknown. According to whether the water-suspended clusters are large or small on the scale of the wavelength ( $1000 \text{ \AA}$ ), two strategies can be followed to evaluate the clustering effect.

### A. Large clusters

We shall first consider the case where the clusters have micrometer sizes, i.e., much larger than the  $\pi$ -plasmon wavelength. The absorption should then be viewed as a bulk phenomenon governed by the complex dielectric function of the clustered particles. We shall assume that the latter form a compact fcc aggregate of identical multishells of density  $n = 4/a^3$ , where  $a = 2\sqrt{2}R$  is the fcc cube edge. We can then construct the bulk dielectric function by writing the Clausius-Mosotti formula<sup>32</sup>

$$\epsilon_c(\omega) = \epsilon_m [1 + z/(1 - z/3)],$$

where  $z(\omega) = n\alpha(\omega)/\epsilon_m\epsilon_0$ ,  $\alpha(\omega)$  being the polarizability of an isolated multishell and  $\epsilon_m$  the dielectric constant of the host material. Bulk absorption which is proportional to  $(\omega/c)\text{Im}\sqrt{\epsilon_c(\omega)}$  takes place in the  $\pi$ -plasmon polariton gap

$$\omega_\pi(1 - n\alpha_0/3\epsilon_0)^{1/2} \leq \omega \leq \omega_\pi(1 + 2n\alpha_0/3\epsilon_0)^{1/2},$$

where  $\omega_\pi$  is the peak absorption frequency of an isolated multishell and  $\alpha_0$  is its static dipole polarizability. The

maximum absorption should occur near the lower end of the gap, where  $\epsilon_c(\omega)$  tends to diverge ( $z \approx 3$ ), i.e., at a position considerably redshifted with respect to the isolated multishell case.

Two cases have to be envisaged depending on whether or not water is excluded from the space between the multishells in the clusters. Since the surface tensions of water and of the graphite basal surface are very similar ( $\sim 0.07$  J/m<sup>2</sup>), it is difficult to decide whether or not water does wet the multishells and percolate throughout the clusters. In the first case (dry clusters), the multishell polarizability  $\alpha(\omega)$  to be used in the Clausius-Mosotti formula is that of a multishell in vacuum. In the second case (wet cluster),  $\alpha(\omega)$  must be the polarizability of an isolated multishell in water as in Fig. 3(b). Figures 5(a) and 5(b) gather the results obtained in various situations.

We first note that the curves of Fig. 5(a) that represent the position of maximum absorption all converge towards a single point when  $r/R \rightarrow 1$ , as if neither the water background nor the clustering had any effect on the  $\pi$ -plasmon absorption of very thin multishells. This is an immediate physical consequence of the fact that, in this limit, the multishells have a vanishing volume and hence a vanishing oscillator strength which effectively decouples them from any environment and from each other.

Figures 5(a) and 5(b) confirm that multishell clustering into micrometer-sized particles has massive redshifting and broadening effects on the absorption peak. The dry-cluster curve [the circles in Fig. 5(a)] now has its plateau around 5.6 eV. The 5.7-eV interstellar hump is bracketed by the results of the isolated multishells [reproduced by the squares in Fig. 5(a)] and the micrometer-sized dry

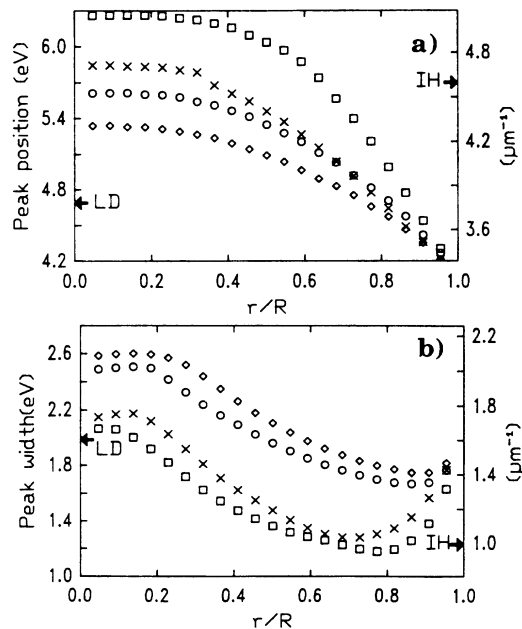


FIG. 5. Absorption peak (a) position and (b) width versus  $r/R$  for a single multishell in vacuum ( $\square$ ), a dry multishell cluster ( $\circ$ ), a single multishell in water ( $\times$ ), and a wet multishell cluster ( $\diamond$ ). The arrows marked IH indicate the average data of the interstellar hump (Ref. 26). The arrows marked LD indicate the laboratory data for hyperfullerenes in water (Ref. 16).

clusters (circles). Could it be that the interstellar dust contains multishell clusters of intermediate size or density (as would be expected for fluffy aggregates due, e.g., to irregular multishell radii  $R$  or polyhedral shapes)? The corresponding widths in the plateau region [ $0 \leq r/R \leq 0.5$  in Fig. 5(b)] do show strong variability but are twice as large as the average width of the interstellar absorption hump indicated by the arrows marked IH. The wet-cluster curve [Fig. 5(a), diamonds] predicts a peak being centered at  $4.1 \mu\text{m}^{-1}$  for  $r/R \approx 0.6$ , i.e., quite close to the observed  $3.8 \mu\text{m}^{-1}$ .<sup>16</sup> Assuming that water does indeed percolate through the suspended particles, it is remarkable that the combined clustering and water effects reduce considerably the dependence of the position of maximum absorption on the parameter  $r/R$  and, simultaneously, bring the range of peak positions and widths within the observed values indicated by the arrow marked LD in Fig. 5.

The effect of clustering is further illustrated in Fig. 3, where curve (c) shows the absorption efficiency of a wet cluster of carbon multishells, whereas curve (b) is for noninteracting particles. Curve (d) is curve (c) redshifted by  $0.3 \mu\text{m}^{-1}$  so as to make its peak position coincide with the observed one. One can see that the peak now has the correct width ( $1.6 \mu\text{m}^{-1}$ ). The residual  $0.3\text{-}\mu\text{m}^{-1}$  redshift between curves (c) and (a) in Fig. 3 remains unexplained. We consider that, given the extreme simplicity of our spherical dielectric model, it would be unreasonable to expect better agreement between theory and experiment.

## B. Small clusters

In the opposite size limit where the clusters comprise but a few multishells, the absorption of each individual cluster must be calculated, e.g., as in Refs. 29 and 30 where the effect of clustering on the infrared optical properties of small particles has been studied in the nonretarded approximation. The model, applied in these papers to NiO soot, was designed to study the dipole-dipole interaction between touching dielectric spherical particles arranged in a large variety of cluster shapes whose sizes were much smaller than the wavelength. A similar strategy could be developed for the present problem since our multishells are also described as polarizable dielectric spheres.

A cluster comprising  $N$  multishells will have its  $3N$  resonance frequencies given by<sup>29</sup>

$$\omega_\mu = \omega_0 (1 + f \lambda_\mu / \epsilon_m)^{1/2}. \quad (8)$$

The  $\lambda_\mu$ 's are the  $3N$  eigenvalues of a real symmetric matrix  $\mathbf{T}$  whose nondiagonal elements are the  $3 \times 3$  dipolar tensors

$$\mathbf{T}_{ij} = (1 - 3\mathbf{R}_{ij}^0 \mathbf{R}_{ij}^0) / (R_{ij}/R)^3$$

constructed from all the vectors  $\mathbf{R}_{ij}$  separating pairs of multishells ( $i, j = 1, \dots, N$ ) and the diagonal elements are zero.  $\mathbf{R}_{ij}^0$  is the unit vector in the  $\mathbf{R}_{ij}$  direction and  $R$  is the radius of the polarizable sphere. In Eq. (8),  $\omega_0$  is the resonance frequency of the isolated multishell and  $f$  stands for the dimensionless static polarizability

$\alpha(0)/4\pi\epsilon_0R^3$ , i.e., the  $l=1$  term of Eq. (5) at low frequency. The  $\lambda_\mu$ 's are real, dimensionless numbers which depend only on the cluster geometry and which are distributed in the range  $-\pi/3\sqrt{2} \leq \lambda_\mu \leq 2\pi/3\sqrt{2}$  (the polariton gap of a large cluster discussed above). Only a limited number of eigenvalues are of interest here, namely, those which correspond to optically active polarization eigenmodes of the cluster.<sup>29</sup> The optical strength (normalized to the unit sphere absorption) of each mode  $\lambda_\mu$  is  $A_\mu = |\sum_i \mathbf{q}_i^\mu|^2$ , where the  $(\mathbf{q}_i^\mu)$  are the normalized eigenvectors of  $\mathbf{T}$  (a single sphere is taken to have unit absorption strength). So, each cluster  $c$  is described, at the dipolar level, by its characteristic "comb"  $\{\lambda_\mu, g_\mu, A_\mu\}_c$ , where  $g_\mu$  is the mode multiplicity. The absorption spectrum of the multishell suspension is then given by the statistical average

$$A(\omega) = \sum_c p_c \sum_\mu g_\mu A_\mu \delta(\omega - \omega_\mu), \quad (9)$$

where the  $p_c$ 's describe the cluster probability distribution and where the  $\delta$  functions are broadened to Lorentzians of width  $\gamma_\mu$ .

For illustration purposes, we shall only show here the active modes of a pair, an equilateral triplet, and a tetrahedron of multishells, as the simplest one-dimensional (1D), two-dimensional (2D), and three-dimensional (3D) clusters, respectively. The corresponding "combs" are listed in Table I. The average absorption of Eq. (9) is shown in Fig. 6, assuming  $p_c = 1$ , successively for the three cases mentioned above and the width of each cluster mode is taken as  $\hbar\gamma_\mu = 1.3$  eV, i.e., of the same order as that of an isolated particle. One sees from Table I that, for each configuration, there are redshifted and blueshifted resonance frequencies but the net absorption band is redshifted as compared to the isolated multishells. This shift is, however, far too small as compared to the observed  $0.5\text{-}\mu\text{m}^{-1}$  offset in Fig. 3 [between curves (a) and (b)].

The van der Waals cohesion energy calculations,<sup>22</sup> i.e., the zero-point energy shift due to aggregation, requires higher multipolar (up to  $l=5$ ) terms. Considering these

TABLE I. Optically active modes for different geometry of small-size polarizable sphere aggregates. The first column gives the multiplicity and the second column, the oscillator strength relative to the single sphere absorption. In columns three and four, the eigenvalues  $\lambda_\mu$  and the corresponding resonance frequencies  $\omega_\mu$  are listed. The last column gives the maximum of the absorption cross section  $\bar{\omega}_0$  when  $\delta$  functions are broadened to Lorentzians of width  $\hbar\gamma_\mu = 1.3$  eV (see Fig. 6). The resonance energy  $\hbar\omega_0$  of an isolated multishell was fixed at 5.25 eV.

	$g_\mu$	$A_\mu$	$\lambda_\mu$	$\omega_\mu$	$\bar{\omega}_0$
Pair	1	2.0	-0.250	5.12	5.21
	2	2.0	0.125	5.32	
Triplet	1	3.0	0.250	5.38	5.20
	2	2.17	-0.241	5.12	
	2	0.83	0.178	5.34	
Tetrahedron	3	2.23	-0.236	5.12	5.19
	3	1.77	0.298	5.40	

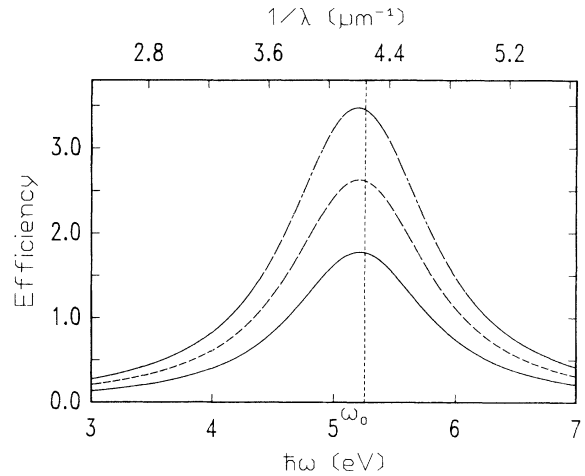


FIG. 6. Absorption efficiency for clusters of  $N=2$  (solid curve), 3 (dashed curve), and 4 (dot-dashed curve) touching graphitic multishells.

terms in the interaction between the multishells, the total dipole resonance is again redshifted but by an amount which is found to be rather small.<sup>33</sup> Clearly, further experimental (other solvent or growth conditions) and theoretical works are needed to distinguish the relative influence of multishell clustering and that of the solvent. We conclude that clustering into aggregates that are small compared to the  $\pi$ -plasmon wavelength cannot explain the observed residual redshift.

## VI. ELECTRON-ENERGY-LOSS SPECTROSCOPY

Finally, we want to briefly discuss the UV optical properties of multishells as they could further be investigated by means of spatially resolved EELS. This technique, combined with scanning transmission electron microscopy (STEM), has been demonstrated<sup>17</sup> in the past ten years to be capable of performing a local analysis of the excitation processes of a target by fast electrons. The spatial resolution is such that one single nanoscopic particle ( $\sim 10$  nm size) can be scanned by varying the impact parameter of the narrow electron beam ( $\sim 1$  nm size) with respect to the particle center.

The theory of the excitation process of a spherical dielectric target has also been developed by a number of authors<sup>34</sup> so that we can directly use the existing formulas to discuss the EELS spectra of individual multishells. We shall restrict our calculations to the case where the impact parameter is larger than the multishell radius. This is because, for that case, the only theoretical quantities required are just the multipolar polarizabilities of the particle which we have established in Eq. (5). The case where the electron beam penetrates the particle is much more complicated and requires the correct treatment of the "begrenzung effect"<sup>34,35</sup> which expresses a sum rule of the relative scattering probabilities by bulk and surface excitations.<sup>35</sup> While this effect is included in the dielectric theory of EELS by isotropic spheres,<sup>34</sup> it has not yet been explored for the special type of "spherically uniaxial" anisotropy exhibited by our multishell model.<sup>36</sup>

When the electron beam travels outside the particle,<sup>34</sup> bulk modes are not excited and the EELS spectrum  $P(\omega)$  involves only the surface modes of multipolar order  $(l, m)$  via the particle dynamic polarizabilities, according to the formula given by Echenique, Howie, and Wheatley:<sup>34</sup>

$$P(\omega) = \sum_{l \geq 1} C_l \text{Im}[\alpha_l(\omega)/4\pi\epsilon_0 R^{2l+1}], \quad (10)$$

where  $\alpha_l(\omega)$  is the multipolar polarizability and the coefficient  $C_l$  are given by

$$C_l = (e^2 R / \pi^2 \epsilon_0 h^2 v^2) (\omega R / v)^{2l} \times \sum_m (2 - \delta_{m,0}) K_m^2(\omega b / v) [(l-m)!(l+m)!], \quad (11)$$

where  $e$  is the electron charge,  $v$  the electron velocity,  $b$  the impact parameter, and  $K_m$  is a cylindrical Bessel function of the second kind.

Figure 7 shows the EELS spectrum computed for a dielectric multishell with an inner radius  $r$  equal to the  $C_{60}$  radius and for incident-electron kinetic energy of 100 keV and 110 Å as impact parameter (the sphere radius is still 100 Å). This example is meant to illustrate what could be observed by EELS of a single multishell of the type observed by Iijima<sup>5</sup> and Ugarte.<sup>6</sup>

One can clearly see two loss features associated again with the  $\pi$ -plasmon (around 6 eV) and the  $\sigma$ -plasmon (around 15 eV) excitations. As in the optical spectrum, due to the large damping, the multiresonance structure gives rise to a single feature in the energy-loss spectrum. The relative intensity of the two peaks ( $\pi$  and  $\sigma$ ) is, however, reversed with respect to the absorption spectrum (see Fig. 3 of Ref. 14) and is in qualitative agreement with EELS experiments on  $C_{60}$  molecules in the gas phase.<sup>37</sup> Since our macroscopic model does not describe correctly

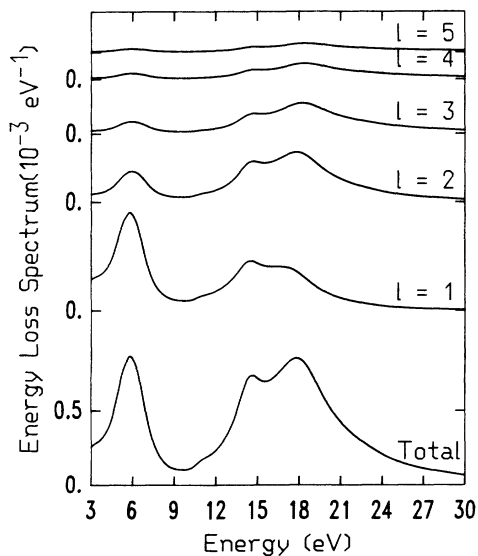


FIG. 7. Electron-energy-loss spectrum of an isolated multishell ( $r = 3.5$  Å,  $R = 100$  Å) for 100-keV electron with impact parameter  $b = 110$  Å. The contribution of the first five multipolar-order terms are shown.

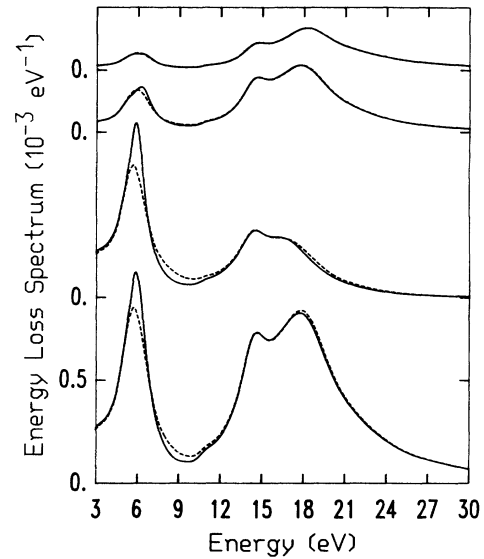


FIG. 8. Same as in Fig. 7 for  $r = 40$  Å (solid curves). The dashed curves illustrate the effects of filling the inner cavity of the multishells with gold.

a single-shell fullerene ( $C_{60}$ ) and since we take account only of losses due to collective motions of the electrons, detailed structures are not expected to closely correspond to experiment on  $C_{60}$ .

We note that multipolar terms contribute significantly up to  $l = 4$ . The expected evolution of multipolar relative strengths is observed: increasing the impact parameter and the kinetic energy enhances the relative weight of the dipolar term.

The solid curve of Fig. 8 shows the EELS spectrum for a multishell with an inner radius of 40 Å. The overall shape of the loss spectrum is very similar to the previous one apart from a narrower width of the  $\pi$ -plasmon peak. The dashed curve is the loss spectrum of the same particle with Au filling the inner cavity (the dielectric properties of Au were taken from Ref. 38). No drastic change is observed due to the presence of this material. One observes a decrease of the  $\pi$ -plasmon resonance intensity, but hardly any change elsewhere. This is due to the assumed impact parameter being larger than the particle radius, so that the electrons are not very sensitive to the innermost structure of the multishell. Since experimental STEM loss spectra are not available for comparison, we do not believe it would be useful to discuss in further detail our theoretical spectra.

## VII. CONCLUSIONS

In this paper we have elaborated a dielectric model of hollow graphitic multishells of nanoscopic size. The model which uses the observed planar graphite optical constants was introduced previously<sup>14</sup> to discuss the 2175-Å absorption hump of interstellar carbon dust. The model is further exploited here in an attempt to interpret new laboratory absorption data on synthetic multishell soot<sup>16</sup> in the  $\pi$ -plasmon spectral region around 6 eV. We

find that single, isolated multishells with graphitic properties cannot fully explain the laboratory observations. Including the effects of multishell clumping does improve the agreement between calculated and measured  $\pi$ -plasmon line shapes. Uncertainty in the dielectric data of graphite is a possible source of unreliability of the computed absorption bands, but this has been shown not to affect greatly the general features of the spectra. The residual small disagreement in the peak position is attributed to some unknown degree of nontransferability of the optical properties of graphite from planar geometry to curved graphitic networks with curvature radii in the atomic size range. Finally, we briefly discuss, on the basis of our simple graphitic multishell model, calculated

electron-energy-loss spectra which could be obtained by STEM operated in the spatially resolved EELS mode and applied to individual multishells.

#### ACKNOWLEDGMENTS

The authors are grateful to Dr. D. Ugarte for many helpful discussions on the subject of graphitic multishells. We thank Professor B. T. Draine for providing us with his compilation of the graphitic dielectric data<sup>19</sup> used in the present work. This work was funded by the national program of the Interuniversity Research Project on Interface Sciences (PAI/IUAP No. 49).

- <sup>1</sup>H. W. Kroto, J. R. Heath, S. C. O'Brien, R. F. Curl, and R. E. Smalley, *Nature* **318**, 162 (1985).
- <sup>2</sup>W. Kratschmer, L. D. Lamb, K. Fostiropoulos, and D. R. Huffman, *Nature* **347**, 354 (1990).
- <sup>3</sup>S. Iijima, *J. Cryst. Growth* **50**, 675 (1980); *J. Phys. Chem.* **91**, 3466 (1987).
- <sup>4</sup>P. P. K. Smith and P. R. Buseck, *Science* **212**, 323 (1981).
- <sup>5</sup>S. Iijima, *Nature* **354**, 56 (1991).
- <sup>6</sup>D. Ugarte, *Nature* **359**, 707 (1992).
- <sup>7</sup>A. A. Lucas, P. Lambin, and R. E. Smalley, *J. Phys. Chem. Solids* **54**, 587 (1993).
- <sup>8</sup>J. P. Hare and H. W. Kroto, *Acc. Chem. Res.* **25**, 106 (1992).
- <sup>9</sup>L. Becker, G. D. McDonald, and J. L. Boda, *Nature* **361**, 595 (1993).
- <sup>10</sup>T. P. Stecher, *Astrophys. J.* **142**, 1693 (1965).
- <sup>11</sup>B. T. Draine, in *Interstellar Dust*, edited by L. J. Allamandola and G. M. M. Tielens (Kluwer, Dordrecht, 1989), p. 313.
- <sup>12</sup>E. L. Wright, *Nature* **336**, 327 (1988).
- <sup>13</sup>R. Rabilizirov, *Astrophys. Space Sci.* **125**, 331 (1986).
- <sup>14</sup>L. Henrard, A. A. Lucas, and P. Lambin, *Astrophys. J.* **406**, 92 (1993).
- <sup>15</sup>P. Apell, D. Östling, and G. Mukhopadhyay, *Solid State Commun.* **87**, 219 (1993).
- <sup>16</sup>W. A. de Heer and D. Ugarte, *Chem. Phys. Lett.* **207**, 480 (1993). We are grateful to these authors for allowing us to reproduce the spectrum of Fig. 3.
- <sup>17</sup>D. Ugarte, C. Colliex, and P. Trebia, *Phys. Rev. B* **45**, 4332 (1992).
- <sup>18</sup>C. F. Bohren and D. R. Huffman, *Absorption and Scattering of Light by Small Particles* (Wiley, New York, 1983).
- <sup>19</sup>B. T. Draine and H. M. Lee, *Astrophys. J.* **285**, 89 (1984).
- <sup>20</sup>D. Ugarte, *Chem. Phys. Lett.* **209**, 99 (1993).
- <sup>21</sup>L. Henrard *et al.* (unpublished).
- <sup>22</sup>P. Lambin, A. A. Lucas, and J. P. Vigneron, *Phys. Rev. B* **46**, 1794 (1992).
- <sup>23</sup>P. Lambin and A. A. Lucas, in *Electronic Properties of High-Temperature Superconductors*, edited by H. Kuzmany, M. Mehring, and J. Fink (Springer, Berlin, 1992), p. 507.
- <sup>24</sup>A. S. Webster, *Astron. Astrophys.* **257**, 750 (1992).
- <sup>25</sup>A. A. Lucas, G. Gensterblum, J. J. Pireaux, P. A. Thiry, R. Caudano, J. P. Vigneron, and P. Lambin, *Phys. Rev. B* **45**, 13 964 (1992); G. Gensterblum, J. J. Pireaux, P. A. Thiry, R. Caudano, J. P. Vigneron, P. Lambin, and A. A. Lucas, *Phys. Rev. Lett.* **67**, 2171 (1991).
- <sup>26</sup>E. L. Fitzpatrick and D. M. Massa, *Astrophys. J.* **306**, 286 (1986).
- <sup>27</sup>M. R. Querry, D. M. Weiliczka, and D. J. Seglestein, in *Handbook of Optical Constants of Solids II*, edited by D. Palik (Academic, New York, 1991).
- <sup>28</sup>H. J. Hagemann, W. Gudat, and C. Kunz, *J. Am. Opt. Soc.* **65**, 742 (1975).
- <sup>29</sup>P. Clippe, R. Evrard, and A. A. Lucas, *Phys. Rev. B* **14**, 1715 (1976).
- <sup>30</sup>M. Ausloos, P. Clippe, and A. A. Lucas, *Phys. Rev. B* **18**, 7176 (1977).
- <sup>31</sup>F. London, *Zeit. Phys. Chem.* **11**, 222 (1930).
- <sup>32</sup>C. Kittel, *Introduction to Solid State Physics*, 5th ed. (Wiley, New York, 1976).
- <sup>33</sup>See J. M. Gérardy and M. Ausloos, *Phys. Rev. B* **22**, 4950 (1980), for a discussion of the effect including quadupolar coupling in the absorption spectrum of clusters of dielectric spheres.
- <sup>34</sup>A recent review is given in P. M. Echenique, A. Howie, and D. J. Wheatley, *Philos. Mag. B* **56**, 335 (1987); see also D. Ugarte, C. Colliex, and P. Trebia, Ref. 17.
- <sup>35</sup>A. A. Lucas and M. Sunjic, *Prog. Surf. Sci.* **2**, 75 (1972).
- <sup>36</sup>L. Henrard *et al.* (unpublished).
- <sup>37</sup>J. W. Kelle and M. A. Coplan, *Chem. Phys. Lett.* **193**, 89 (1992).
- <sup>38</sup>*Handbook of Optical Constants of Solids*, edited by E. D. Palik (Academic, New York, 1985).